



HAL
open science

Impact of the thermal scattering law of H in H₂O on the isothermal temperature reactivity coefficients for UOX and MOX fuel lattices in cold operating conditions

Juan Pablo Scotta, Gilles Noguere, David Bernard, Jose Ignacio Marquez Damian, Alain Santamarina

► To cite this version:

Juan Pablo Scotta, Gilles Noguere, David Bernard, Jose Ignacio Marquez Damian, Alain Santamarina. Impact of the thermal scattering law of H in H₂O on the isothermal temperature reactivity coefficients for UOX and MOX fuel lattices in cold operating conditions. EPJ N - Nuclear Sciences & Technologies, 2016, 2, pp.28. 10.1051/epjn/2016020 . cea-02305894

HAL Id: cea-02305894

<https://cea.hal.science/cea-02305894>

Submitted on 4 Oct 2019

HAL is a multi-disciplinary open access archive for the deposit and dissemination of scientific research documents, whether they are published or not. The documents may come from teaching and research institutions in France or abroad, or from public or private research centers.

L'archive ouverte pluridisciplinaire **HAL**, est destinée au dépôt et à la diffusion de documents scientifiques de niveau recherche, publiés ou non, émanant des établissements d'enseignement et de recherche français ou étrangers, des laboratoires publics ou privés.

Impact of the thermal scattering law of H in H₂O on the isothermal temperature reactivity coefficients for UOX and MOX fuel lattices in cold operating conditions

Juan Pablo Scotta¹, Gilles Noguere^{1*}, David Bernard¹, Jose Ignacio Marquez Damian², and Alain Santamarina¹

¹ CEA, DEN, DER Cadarache, Saint Paul les Durance, France

² Neutron Physics Department and Instituto Balseiro, Centro Atomico Bariloche, CNEA, Bariloche, Argentina

Received: 25 November 2015 / Received in final form: 24 February 2016 / Accepted: 23 March 2016

Abstract. The contribution of the thermal scattering law of hydrogen in light water to isothermal temperature reactivity coefficients for UOX and MOX lattices was studied in the frame of the MISTRAL critical experiments carried out in the zero power reactor EOLE of CEA Cadarache (France). The interpretation of the core residual reactivity measured between 6 °C to 80 °C (by step of 5 °C) was performed with the Monte-Carlo code TRIPOLI4[®]. The nuclear data from the JEFF-3.1.1 library were used in the calculations. Three different thermal scattering laws of hydrogen in light water were tested in order to evaluate their impact on the MISTRAL calculations. The thermal scattering laws of interest were firstly those recommended in JEFF-3.1.1 and ENDF/B-VII.1 and also that recently produced at the atomic center of Bariloche (CAB, Argentina) with molecular dynamic simulations. The present work indicates that the calculation-to-experimental bias is -0.4 ± 0.3 pcm/°C in the UOX core and -1.0 ± 0.3 pcm/°C in the MOX cores, when the JEFF-3.1.1 library is used. An improvement is observed over the whole temperature range with the CAB model. The calculation-to-experimental bias vanishes for the UOX core (-0.02 pcm/°C) and becomes close to -0.7 pcm/°C for the MOX cores. The magnitude of these bias have to be connected to the typical value of the temperature reactivity coefficient that ranges from -5 pcm/°C at Beginning Of Cycle (BOC) up to -50 pcm/°C at End Of Cycle (EOC), in PWR conditions.

1 Introduction

The isothermal temperature reactivity coefficients, or equivalently the reactivity temperature coefficients (RTC), are one of the major reactor safety parameters. They represent the change in reactivity due to a change in temperature [1]. Recent publications deal with RTC for various reactor configurations in “cold conditions” ($T < 50$ °C) [2–4] up to “hot conditions” ($T < 300$ °C) [5,6]. The present work focuses on the calculation of RTC for critical assemblies in “cold conditions” for temperatures ranging from 6 °C to 80 °C at atmospheric pressure. The isothermal temperature coefficient $\alpha_{iso}(T)$ is determined from the excess of reactivity $\rho(T)$ measured at given temperatures T . In practice, the experimental results allow estimating $\Delta\alpha_{iso}(T)$ which represents the calculation error on RTC. The latter is given by the derivative of the difference $\Delta\rho(T)$ between the calculated (C) and measured (E) excess of reactivity with respect to

the temperature:

$$\Delta\alpha_{iso}(T) = \frac{\partial\Delta\rho(T)}{\partial T}, \quad (1)$$

with

$$\Delta\rho(T) = \rho_C(T) - \rho_E(T). \quad (2)$$

A series of MISTRAL experiments [7–15] was carried out in the EOLE facility of CEA Cadarache (France) in order to study $\Delta\alpha_{iso}$ for UOX (MISTRAL-1 configuration) and MOX (MISTRAL-2 and MISTRAL-3 configurations) lattices. Previous interpretations [16,17] were performed with the deterministic code APOLLO2 [18] by using the evaluated nuclear data libraries JEF-2.2 and JEFF-3.1.1. Results are summarized in Table 1. According to conclusions reported in reference [16], $\Delta\alpha_{iso}$ is mainly sensitive to the spectral shift of thermal neutrons in the low temperature range ($T < 40$ °C). The contribution of the water density effects becomes sizeable when the temperature increases. In addition, the contribution of the thermal spectrum effects

* e-mail: gilles.noguere@cea.fr

Table 1. Summary of the calculation errors $\Delta\alpha_{iso}$ for the MISTRAL experiments obtained with the deterministic code APOLLO2 [18] in association with the JEF-2.2 and JEFF-3.1.1 nuclear data libraries [16,17].

MISTRAL configuration	Temperature range	Calculation errors on RTC in pcm/°C	
		JEF-2.2	JEFF-3.1.1
MISTRAL-1 (UOX)	10 to 40 °C	-0.0 ± 0.3	$+0.9 \pm 0.4$
	40 to 80 °C	-0.1 ± 0.4	$+0.1 \pm 0.4$
	10 to 80 °C	-0.0 ± 0.3	$+0.4 \pm 0.3$
MISTRAL-2 (MOX)	10 to 40 °C	-2.0 ± 0.2	-0.5 ± 0.4
	40 to 80 °C	-1.0 ± 0.3	-1.1 ± 0.4
	10 to 80 °C	-1.5 ± 0.2	-0.9 ± 0.3
MISTRAL-3 (MOX)	10 to 40 °C	-2.3 ± 0.3	-0.4 ± 0.5
	40 to 80 °C	-0.8 ± 0.3	-1.4 ± 0.5
	10 to 80 °C	-1.6 ± 0.3	-1.0 ± 0.4

to the calculation errors is strongly dependent on the shape of the ^{235}U and ^{239}Pu neutron cross-sections in the thermal region.

The main physical trends observed in the MISTRAL-1 experiment between 6 °C and 80 °C for UOX lattices are confirmed by a sensitivity analysis performed on the critical assembly of the Kyoto University between 27 °C and 57 °C [19]. However, the reported results mainly emphasise the importance of the thermal scattering cross-section of hydrogen bound to H_2O . Such a significant contribution to the calculation errors $\Delta\alpha_{iso}$ was not reported in the previous interpretations of the MISTRAL programs.

The present work aims at quantifying the impact of the thermal scattering law (TSL) of hydrogen in light water on $\Delta\alpha_{iso}$. Reference values were calculated with the Monte-Carlo code TRIPOLI4[®] [20] by using the evaluated nuclear data library JEFF-3.1.1 [21]. They are compared to results obtained with JEFF-3.1.1 in which the TSL are replaced by those of the US library ENDF/B-VII.1 [22] and of the CAB library [23], produced at the atomic center of Bariloche.

2 Thermal scattering law for light water

2.1 Governing equations

In the low energy range (below approximately 5 eV), the neutron scattering in a light water moderator is affected by the intermolecular and intramolecular hydrogen bonds. They modify the energy and angular distributions of secondary neutrons. A description of the model for water is given in references [24,25], and studies that investigate how we can accurately calculate neutrons slowing down in water are reported in reference [26]. The double differential incoherent inelastic scattering cross-section of a single bound atom in molecule (H bound in H_2O) can be written as a function of the symmetric scattering law $S(\alpha, \beta)$:

$$\frac{\partial^2 \sigma}{\partial \Omega \partial E} = \frac{\sigma_b}{4\pi kT} \sqrt{\frac{E'}{E}} \exp\left(-\frac{\beta}{2}\right) S(\alpha, \beta), \quad (3)$$

where E and E' are the incident and secondary neutron energies, Ω defines the scattering angle, σ_b represents the characteristic bound cross-section for the material, k is the Boltzmann constant and T is the temperature of the material. The scattering law contains all the dynamic and structural information about the target system. It is a function of the momentum transfer α :

$$\alpha = \frac{E' + E - 2\sqrt{E'E} \cos(\theta)}{AkT}, \quad (4)$$

and of the energy transfer β :

$$\beta = \frac{E' - E}{kT}, \quad (5)$$

where $\cos(\theta)$ is the cosine of the scattering angle in the laboratory system and A is the ratio of the mass of the scattering atom to the neutron mass.

Some approximations are customarily used to represent the $S(\alpha, \beta)$ function over a large dynamical range with simple mathematical expressions. For hydrogenous moderators, like light water, the incoherent neutron scattering dominates the scattering process. This assumption, combined with the Gaussian approximation [27], leads to the following expression for the scattering law:

$$S(\alpha, \beta) = \frac{1}{2\pi} \int_{-\infty}^{+\infty} e^{i\beta t} e^{-\gamma(t)} dt, \quad (6)$$

where the function $\gamma(t)$ is computed as:

$$\gamma(t) = \alpha \int_{-\infty}^{+\infty} P(\beta) (1 - e^{-i\beta t}) e^{\beta/2} dt. \quad (7)$$

The function $P(\beta)$ is related to the generalized frequency spectrum of the material $\rho(\beta)$ by:

$$P(\beta) = \frac{\rho(\beta)}{2\beta \sinh(\beta/2)}, \quad (8)$$

with the condition:

$$\int_0^{+\infty} \rho(\beta) d\beta = 1. \quad (9)$$

Table 2. Parameters for the TSL models of H in H₂O at 294 K.

Model parameters		IKE model		CAB model
		JEFF-3.1.1	ENDF/B-VII.1	
Diffusion constant	c	-	-	4.0606
First oscillator energy (meV)	E_1	0.205	0.205	0.205
Second oscillator energy (meV)	E_2	0.436	0.436	0.430
Continuous spectrum weight	ω_c	0.4891	0.4904	0.5224
Translational weight	ω_t	0.0217	0.0192	0.0086
First oscillator weight	ω_1	0.1630	0.1635	0.1563
Second oscillator weight	ω_2	0.3261	0.3269	0.3126

The distribution $\rho(\beta)$ contains a complete description of the intermolecular and intramolecular vibration modes of the water molecule.

2.2 Frequency spectrum used in the TSL models

The frequency spectrum is a continuous probability density function. For H in light water, $\rho(\beta)$ can be decomposed into a sum of four components:

$$\rho(\beta) = \omega_c \rho_c(\beta) + \omega_t \rho_t(\beta, c) + \omega_1 \delta(\beta_{E_1}) + \omega_2 \delta(\beta_{E_2}), \quad (10)$$

where $\rho_c(\beta)$ is a continuous distribution that describes the rotational mode of the water molecule, $\rho_t(\beta, c)$ mimics the translational mode that depends on the diffusion constant c and $\omega_1 \delta(\beta_{E_1}) + \omega_2 \delta(\beta_{E_2})$ is a sum of two discrete oscillators which define the intramolecular vibrations, namely bending and stretching. The weights satisfy the following condition:

$$\omega_c + \omega_t + \omega_1 + \omega_2 = 1. \quad (11)$$

Three different sets of frequency spectra were studied. Two of them stem from the model developed by Mattes and Keinert [28]. This model will be called IKE model in the text. It was used for establishing the thermal scattering laws available in the JEFF-3.1.1 and ENDF/B-VII.1 libraries. The third one, called CAB model [23], was developed by J.I. Marquez Damian at the atomic center of Bariloche. Parameters used in each model at 294 K are given in Table 2.

In the JEFF-3.1.1 library, the frequency spectra of H in H₂O are based on experimental values measured by Page and Haywood at 294 K and 550 K [29]. The symmetric and asymmetric stretching modes are described by a single discrete oscillator at 0.436 eV. For the bending mode, a discrete oscillator at 0.205 eV was used. The IKE model parameters were slightly modified for producing new $S(\alpha, \beta)$ tables for the ENDF/B-VII.1 library. The characteristics of the discrete oscillators remain the same as JEFF-3.1.1.

A new approach was used for the CAB model. Molecular dynamic simulations were performed for calculating the temperature-dependent frequency spectra of hydrogen in light water. The characteristics of the discrete oscillator (energies and weights) obtained from the Molecular dynamic

simulations and used in the IKE model are nearly similar. In contrast, large differences can be observed between the continuous rotational mode used in each model (Fig. 1). For the translational mode ($\omega_t \rho_t$), a diffusion model [30] with an effective mass of 116 a.m.u was adopted in the CAB model, while a free gas model with a mass of 52 a.m.u and 46 a.m.u was used in ENDF/B-VII.1 and in JEFF-3.1.1, respectively. Upon interaction with the incident neutron, a heavier effective mass will reduce the contribution of the translational mode of the water molecule (ω_t decreases) and will increase the probability of undergoing a rotation (ω_c increases). In the CAB model, special attention has been paid to the description of the translational mode for improving the agreement between the experimental and calculated cross-sections in the cold neutron energy range, below the thermal energy of 25.3 meV. The impact of the $S(\alpha, \beta)$ tables generated with each model was investigated in the frame of the MISTRAL program.

3 Interpretation of the MISTRAL programs with the Monte-Carlo TRIPOLI4[®]

3.1 Description of the MISTRAL configurations

The MISTRAL experimental programs were designed in the late nineties to evaluate the feasibility of using 100% MOX fuel in light water reactors. The different core configurations were tested in the EOLE reactor of CEA Cadarache (France). Many relevant neutronic parameters were measured during the MISTRAL programs such as critical mass, geometrical buckling, spectral indices, conversion factor, isothermal temperature coefficient, single absorber worth, soluble boron worth and effective delayed neutron fraction.

The present work focuses on the isothermal temperature reactivity coefficient measured in the MISTRAL-1, MISTRAL-2 and MISTRAL-3 configurations (Fig. 2). A detailed description of the experiments can be found in reference [16].

The MISTRAL-1 core is a homogenous UO₂ configuration that serves as reference for the whole MISTRAL programs. The cylindrical core consists of a regular lattice using 750 standard PWR fuel pins (3.7% enriched in ²³⁵U) in a square pitch of 1.32 cm with 16 guide tubes dedicated for safety rods. The moderation ratio is 1.7 (representative of LWR moderation).

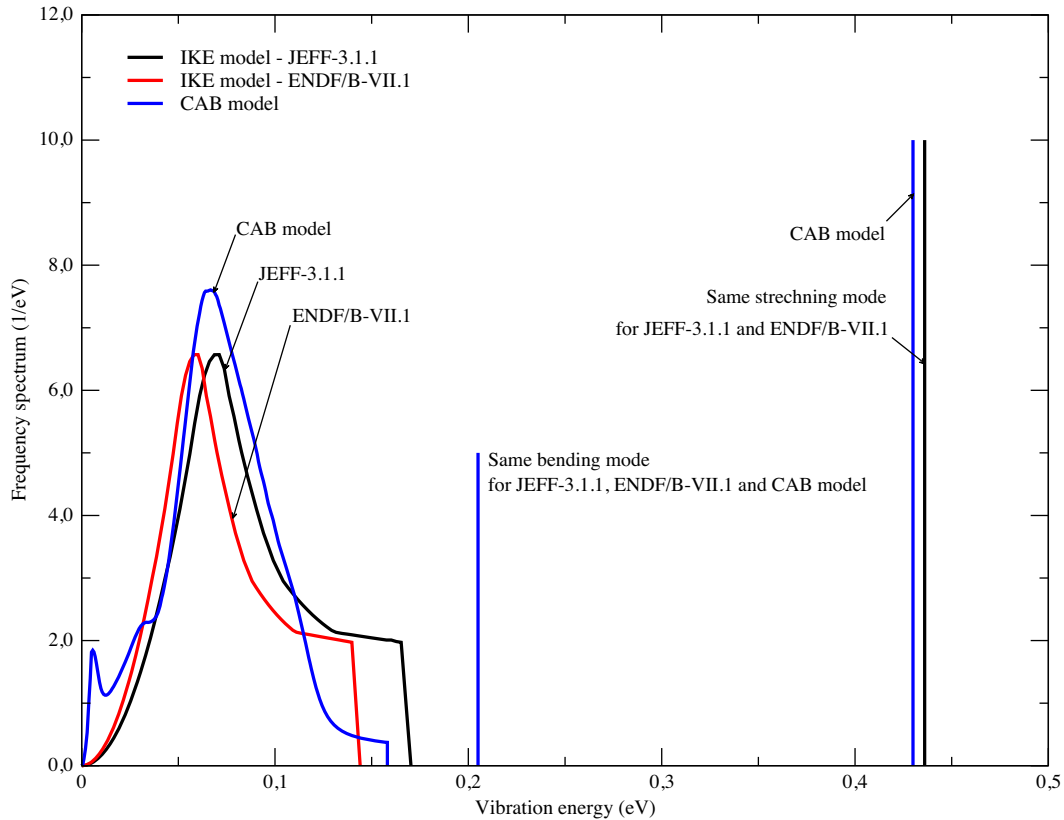


Fig. 1. Comparison of the continuous and discrete frequency spectrum for H in H_2O at 294 K.

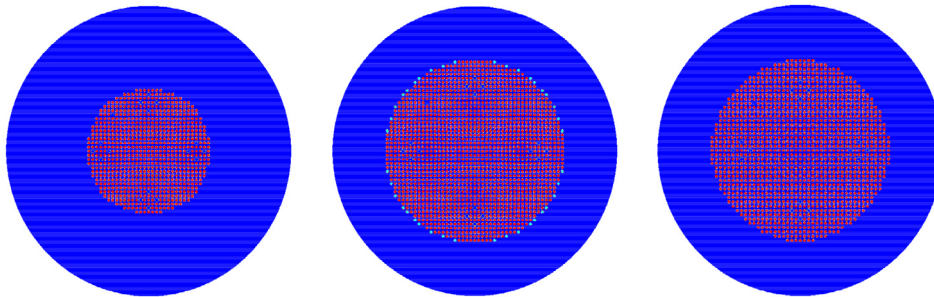


Fig. 2. Radial cross-sections of the MISTRAL-1 (750 UOX fuel pins), MISTRAL-2 (1572 MOX fuel pins) and MISTRAL-3 (1388 MOX fuel pins) cores. For MISTRAL-2, the given core is the configuration at 20 °C.

The MISTRAL-2 core is a homogenous 100% MOX configuration with 1572 MOX fuel pins with a fuel enrichment of 7% in Am-PuO₂. This second configuration is characterized by the same number of guide tubes, pitch and moderation ratio as MISTRAL-1.

The MISTRAL-3 core is a homogenous 100% MOX configuration with 1388 fuel pins with a fuel enrichment of 7% in Am-PuO₂. The main differences with respect to MISTRAL-2 are the moderation ratio, close to 2.1, and the square pitch which was set to 1.39 cm. The aim of this configuration was to measure the fundamental neutronic parameters in a slightly over-moderated lattice.

The reactivity excess was measured as a function of the temperature from 6 °C to 80 °C with a fine temperature step of 5 °C. In the MISTRAL-1 and MISTRAL-3

configurations, the concentration of the soluble boron was adjusted in the moderator in order to compensate the reactivity loss due to the temperature increase. In MISTRAL-2, the criticality was achieved by adjusting the critical size of the core. MOX pins with enrichment of 8.7% were strategically added at the periphery of the core.

3.2 Processing of the TSL data files for TRIPOLI4[®]

The Monte-Carlo code TRIPOLI4[®] [20] was used for the interpretation of the MISTRAL experiments. For this purpose, thermal scattering files of H in H₂O were generated for each temperature step in a format compatible with the official nuclear data library of TRIPOLI4[®] based on JEFF-3.1.1.

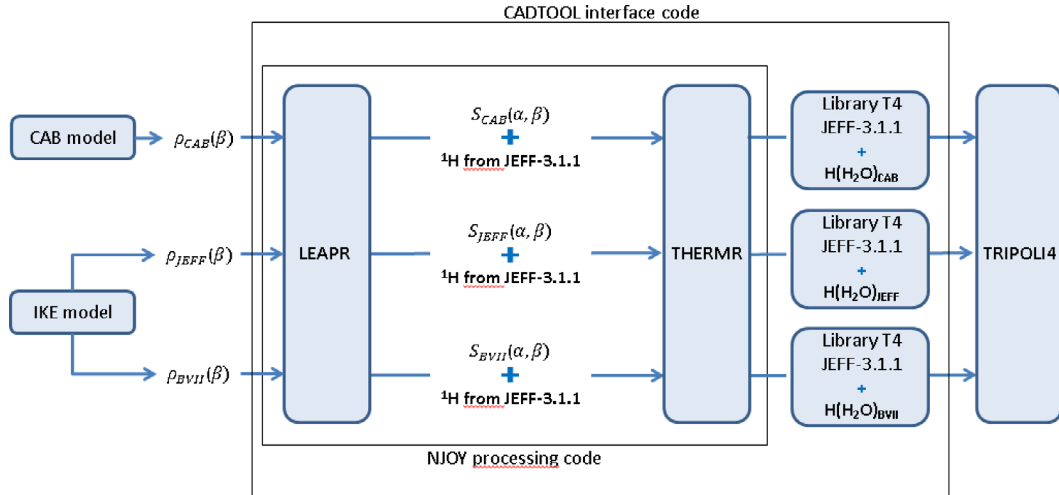


Fig. 3. Flowchart of the calculation scheme used to produce $S(\alpha, \beta)$ tables for the TRIPOLI4[®] code [20]. The processing of the $S(\alpha, \beta)$ tables from the three TSL data files of interest for this work is performed with the NJOY code [25]. The cross-sections of the JEFF-3.1.1 library is used for the neutron transport and only $S(\alpha, \beta)$ of light water are replaced by taking the needed information from alternatively the JEFF-3.1.1, ENDF/B-VII.1 and CAB libraries. The CADTOOL package [31] provides an easy-to-use interface for automated sequential processing schemes.

Table 3. Excess of reactivity calculated with the TRIPOLI4[®] code for the MISTRAL-1 configuration at 20 °C. The differences $C_i - C_1$ are calculated by using the result obtained with the official T4 library as reference.

Thermal scattering law for H in H ₂ O		$C_i - E$	$C_i - C_1$
C_1	Official T4 library based on JEFF-3.1.1	196 ± 10 pcm	–
C_2	H(H ₂ O) of the official T4 library is replaced by ¹ H generated with the Free Gas Model (no THERMR processing)	958 ± 10 pcm	$+762 \pm 14$ pcm
C_3	H(H ₂ O) of the official T4 library is replaced by H(H ₂ O) generated from THERMR	187 ± 10 pcm	-9 ± 14 pcm
C_4	H(H ₂ O) of the official T4 library is replaced by H(H ₂ O) generated from LEAPR+THERMR	186 ± 10 pcm	-10 ± 14 pcm

The processing of the TSL data files was performed with the NJOY code [25]. Two modules of NJOY are specifically dedicated to this treatment. The LEAPR module calculates the $S(\alpha, \beta)$ tables by using the formalism briefly described in Section 2.1. The THERMR module uses the $S(\alpha, \beta)$ tables for calculating the double differential inelastic cross-sections (Eq. (3)). Figure 3 shows the flowchart representing the processing scheme applied to the TSL files of JEFF-3.1.1, ENDF/B-VII.1 and generated with the CAB model.

Before analyzing the MISTRAL experiments, the processing scheme used in this work to produce thermal scattering laws was tested and validated against the official library of TRIPOLI4[®]. The differences on the calculated effective multiplication factor (k_{eff}) between the official library and our NJOY treatment were quantified on the MISTRAL-1 benchmark at 20 °C. Results are reported in Table 3.

As a first step, we have evaluated the sensitivity of the calculated k_{eff} to the thermal scattering law of hydrogen by considering the hydrogen in water as a free gas. Figure 4 compares the ¹H and H in H₂O total cross-sections calculated at $T = 300$ K. The thermal energy cut-off is equal to 4.95 eV. Then, TRIPOLI4[®] uses the Sampling of

the Velocity of the Target nucleus (SVT) up to $T_{\text{max}} = 400k_B T$. Beyond this energy, the static Asymptotic Kernel (AK) approximation is applied. The importance of the TSL depends on the size of the neutronic core. A small core yields a high thermal neutron leakage, so a high effect of the thermal neutron models is expected. In our case, the free gas model overestimates the experimental reactivity excess by approximately +800 pcm. Such a large difference confirms the importance of the thermal scattering laws and their processing with the LEAPR and THERMR modules of the NJOY code for a correct interpretation of the MISTRAL experiments.

The two NJOY modules were tested separately. The THERMR module was applied to the $S(\alpha, \beta)$ tables given with the official TRIPOLI4[®] library. In order to test the compatibility of the LEAPR calculations, we used the input files for H in H₂O reported by Mattes and Keinert in reference [28]. The input file contains the model parameters listed in Table 2 and the continuous frequency spectra shown in Figure 1. As reported in Table 3, the differences between the k_{eff} values calculated with the TSL files coming from our processing scheme and the official library of

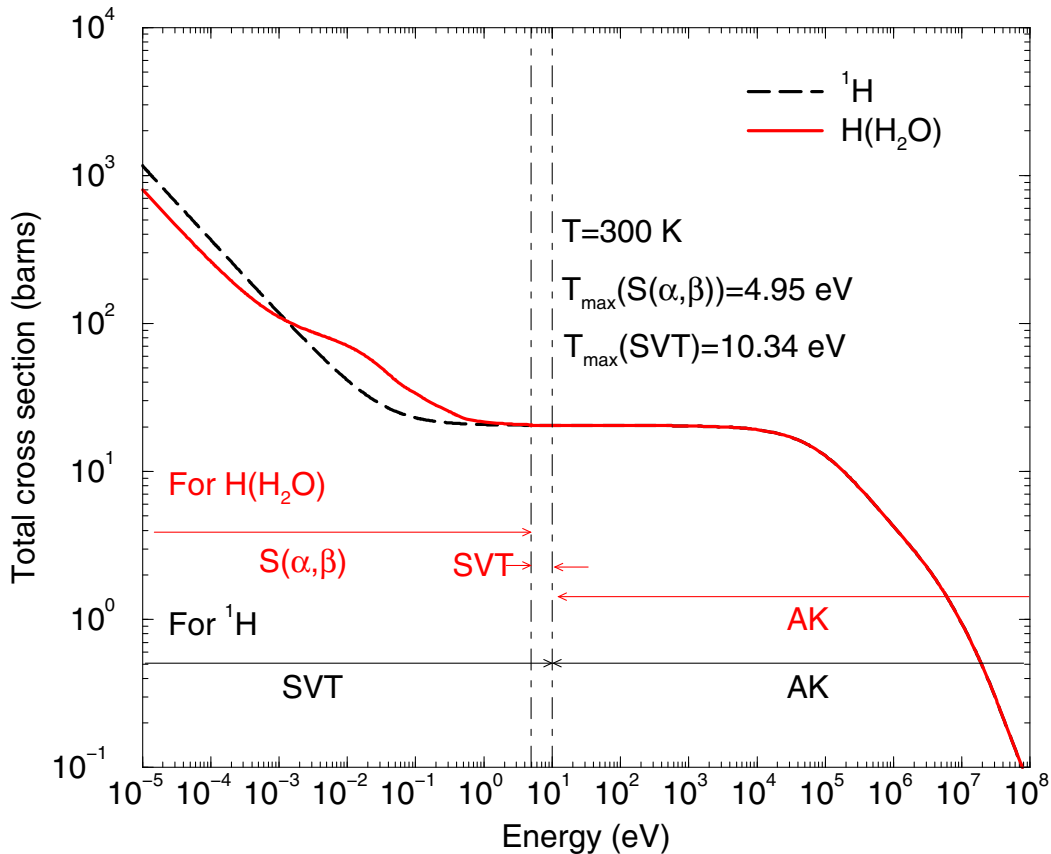


Fig. 4. Comparison of the ^1H and H in H_2O total cross-sections calculated at $T = 300$ K. The thermal energy cut-off is equal to 4.95 eV. Then, TRIPOLI[®] uses the Sampling of the Velocity of the Target nucleus (SVT) up to $T_{\max} = 400k_B T$. Beyond this energy, the static Asymptotic Kernel (AK) approximation is applied.

TRIPOLI[®] are negligible and remain below the statistical uncertainties of ± 10 pcm. This good agreement shows that our processing scheme can be safely used for the interpretation of the MISTRAL programs.

3.3 Interpolation of the model parameters

In the JEFF-3.1.1 and ENDF/B-VII.1 libraries, the thermal scattering laws are tabulated in terms of $S(\alpha, \beta)$ tables over a broad temperature mesh. Only three (20 °C, 50 °C and 100 °C) and two (20 °C and 77 °C) temperatures, respectively, are reported to map the temperature range of the MISTRAL programs from 6 °C to 80 °C. Such a broad temperature mesh is not adequate for a precise estimation of the isothermal temperature reactivity coefficient at room temperature.

New $S(\alpha, \beta)$ tables were generated up to 80 °C with a fine temperature step of 5 °C by interpolating the model parameters and the frequency spectra contained in the LEAPR input files. Results for parameters established by Mattes and Keinert [28] are shown in Figures 5 and 6. The total cross-sections of H in H_2O from the JEFF-3.1.1 library are compared in Figure 7 to the total cross-sections calculated with a fine temperature mesh. High sensitivities to the temperature are observed for cold neutrons ($E < 25.3$ meV).

Final results were verified by comparing the total cross-section reconstructed from our interpolation procedure to the JEFF-3.1.1 total cross-section evaluated at 20 °C and 50 °C. In both cases, the differences remain negligible over the neutron energy range of interest. They reach a maximum of 1.5 barns at 0.01 meV, corresponding to a calculation error of 0.15%.

4 Results and discussions

4.1 Comparison of the TSL data files

The processing scheme used in association with our interpolation procedure allows comparing the thermal scattering laws for each temperature of the MISTRAL programs up to 80 °C. For the sake of clarity, we only report comparison on the total cross-sections in Figure 8.

In the cold neutron energy range, large discrepancies are observed between the TSL of JEFF-3.1.1, ENDF/B-VII.1 and established with the CAB model. The discrepancies slightly decrease when the temperature increases. In the CAB model, the use of diffusion instead of free gas for molecular translation allows to better reproduce the experimental data measured below 1 meV. Detailed comparisons with experimental data are given in reference [23].

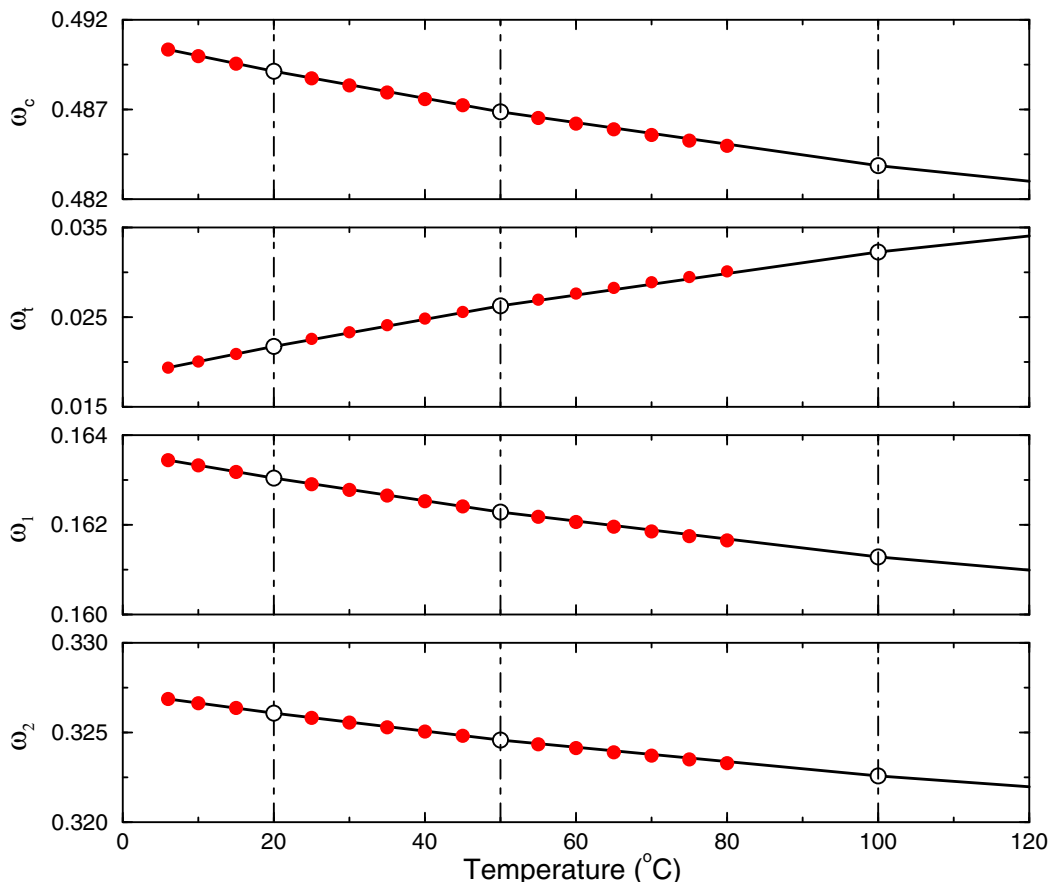


Fig. 5. Interpolation of the model parameters established by Mattes and Keinert [28] between 6 °C to 80 °C. The meaning of each parameter is given in Table 2.

In the thermal energy range, the magnitude of the differences does not change over the temperature range between 6 °C to 80 °C. The discrepancies between JEFF-3.1.1 and the CAB model reach $\approx 5\%$ at 25.3 meV. In the case of ENDF/B-VII.1, the discrepancies remain smaller or equal to 2.5%.

4.2 Reactivity excess as a function of temperature

The interpretation of the three MISTRAL configurations was performed with the JEFF-3.1.1 library. As shown in the flowchart of Figure 3, we have only replaced the thermal scattering laws of H in H₂O by those calculated with the processing scheme presented in Sections 3.2 and 3.3. Results reported in Table 4 represent the differences in reactivity $\Delta\rho(T)$, where Δ indicates the deviation from the experimental values. Contributions of the experimental uncertainties and those coming from the Monte-Carlo calculations are taken into account separately. For each configuration the statistical uncertainty due to the Monte-Carlo calculations is close to ± 2 pcm. The experimental uncertainties account for uncertainties that mainly come from the kinetic parameters, the measurements of the doubling time and of the boron concentration. The final experimental uncertainty ranges from ± 10 pcm to ± 25 pcm. In the present work, the contribution of the kinetic parameters to the final uncertain-

ty is small because we have used β_{eff} values which have been measured during the MISTRAL-1 and MISTRAL-2 programs. Results reported in reference [32] are 788 ± 12 pcm for MISTRAL-1 (UOX core) and 370 ± 6 pcm for MISTRAL-2 (MOX core). Technological uncertainties are not included. For the EOLE facility, the magnitude of such uncertainties is close to ± 200 pcm.

The top plot of Figure 9 shows the $\Delta\rho(T)$ values obtained for the MISTRAL-1 experiment as a function of the temperature. Using the JEFF-3.1.1 library, we observe a slight overestimation of the core reactivity (+192 pcm at 20 °C). Compared to JEFF-3.1.1, the thermal scattering laws of ENDF/B-VII.1 and those from the CAB model increase the calculated reactivity by respectively +65 pcm and +100 pcm on average.

The middle and bottom plots of Figure 9 show the $\Delta\rho(T)$ values obtained for the MISTRAL-2 and MISTRAL-3 experiments. Using the JEFF-3.1.1 library, the MISTRAL-2 core reactivity is overestimated by +732 pcm at 20 °C. As for MISTRAL-1, the calculated reactivity increases when the thermal scattering laws of ENDF/B-VII.1 and those from the CAB model are used. For MISTRAL-2, the mean differences are +80 pcm and +180 pcm respectively. Similar trends are obtained for MISTRAL-3 (+60 pcm and +140 pcm). Larger differences are reached because MOX fuel calculations are more sensitive to the thermal scattering laws of hydrogen in light water. One of the relevant results is

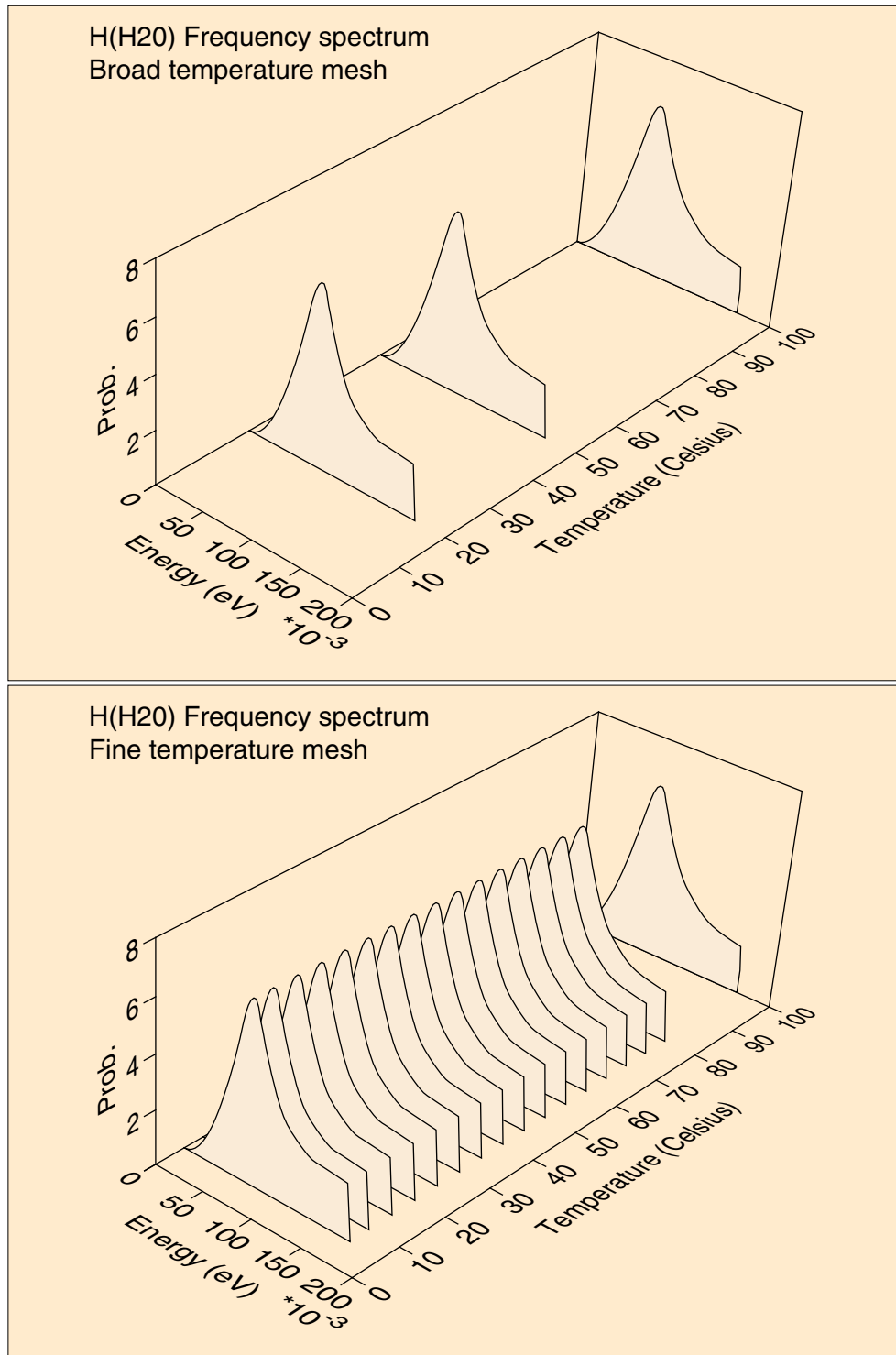


Fig. 6. Continuous frequency spectra for H in H₂O for the broad temperature mesh of the JEFF-1.1.1 library (top plot) and interpolated over a fine temperature mesh (bottom plot).

the sizeable overestimation of the experimental reactivity by the calculations. It reaches $\Delta\rho \approx 900$ pcm when the thermal scattering laws calculated with the CAB model are used. Such an integral trend could be attributed to the americium cross-sections. New experimental works seem to indicate

that the thermal capture cross-section and the capture resonance integral of ²⁴¹Am could be overestimated in JEFF-3.1.1 by 15% and 20%, respectively [33]. A new ²⁴¹Am evaluation was included in the latest version of the JEFF library (JEFF-3.2) for improving the calculations of the k_{eff}

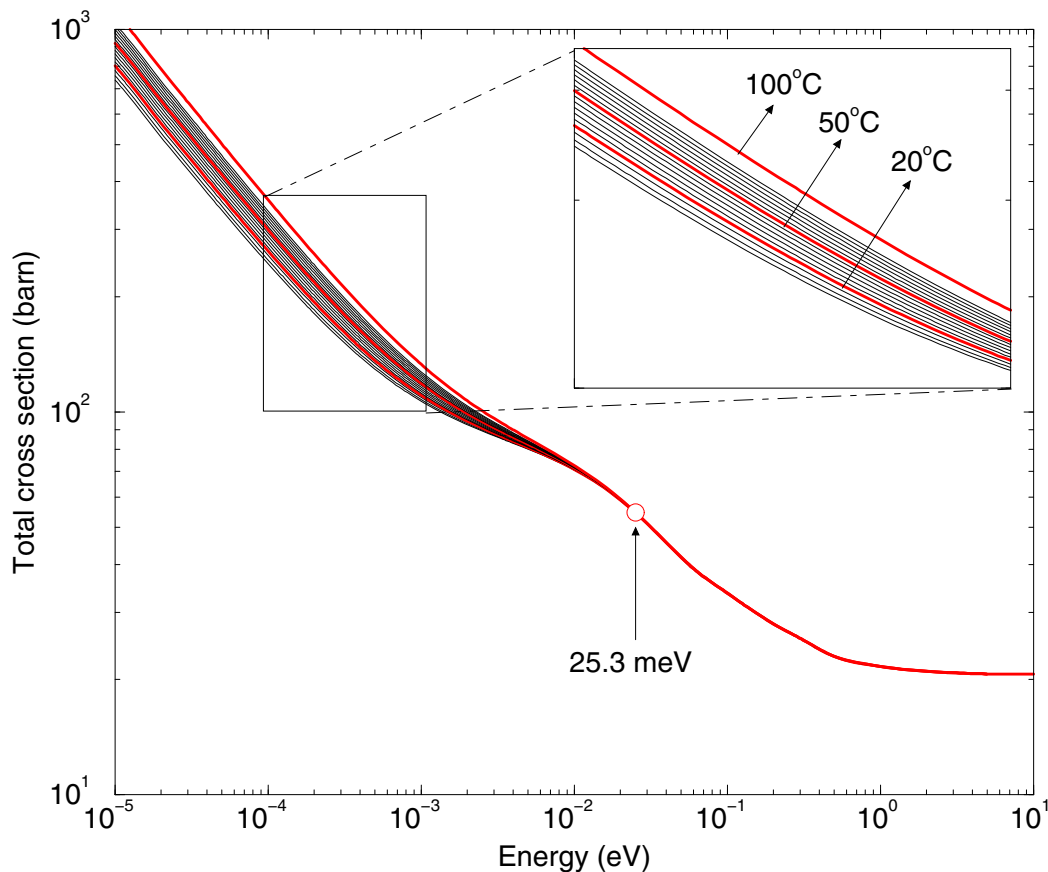


Fig. 7. Total cross-section of H in H₂O calculated with the broad temperature mesh of the JEFF-1.1.1 library (20 °C, 50 °C and 100 °C) and interpolated over a fine temperature mesh (from 6 °C to 80 °C).

values [34]. In the case of the MISTRAL programs, this new ²⁴¹Am evaluation provides improved $\Delta\rho$ values at room temperature ranging from 200 pcm to 300 pcm [35].

Each component of the frequency spectrum (Eq. (10)) was investigated in order to understand the origin of the increase of the reactivity (few tens of pcm) when the ENDF/B-VII.1 and CAB models are used. This increase can be explained by two competitive behaviors, which can be observed in Figure 8. The increase of the calculated reactivity is mainly connected to the decrease of the total cross-section between 0.01 eV and 1 eV, which is partially compensated by an increase of the total cross-section between 0.001 eV and 0.01 eV. Above 0.01 eV, the total cross-section is driven by the continuous part of the frequency spectrum $\rho_c(\beta)$ (Fig. 1), indicating that the intermolecular vibrations have a major contribution in the transport of neutrons in the moderator.

To obtain a curve of the excess reactivity as a function of the temperature in units of degree Celsius, results in pcm were fitted with an empirical function. Linear [4], quadratic [19] or cubic [16] polynomials are used in the literature:

$$\Delta\rho(T) = a_0 + \sum_{i=1}^n a_i T^i, \quad (12)$$

where the coefficients a_i are free parameters. In the present work, a systematic study is reported as a function of the degree of the polynomial ($n = 1, 2, 3$). The fitting algorithm of the CONRAD code was used [36]. A Chi-square test provides a measure of the goodness-of-fit. It was used to select the optimal degree of the polynomial. Table 5 reports the final Chi-square values provided by the CONRAD code for $n = 1, 2, 3$. The originality of our work is the simultaneous analysis of the $\Delta\rho(T)$ values calculated for the MISTRAL-2 and MISTRAL-3 programs. The calculations were performed by introducing a free normalization factor which does not change the shape of $\Delta\rho$ as a function of the temperature. This approach aims to provide a global trend for the MOX configurations.

For MISTRAL-1, a quadratic polynomial ($n = 2$) gives a rather good description of the $\Delta\rho(T)$ results. A different trend is observed for MOX fuel. A simple linear fit ($n = 1$) of the MISTRAL-2 and MISTRAL-3 results provides better Chi-square values than a cubic polynomial. Best fit curves are reported in Figure 9. The corresponding polynomial coefficients a_i are given in Table 6. The quoted uncertainties account for the statistical uncertainties in order to quantify the contribution of the Monte-Carlo calculations only. The propagation of the experimental uncertainties was already addressed in the frame of the previous analysis performed with the deterministic code APOLLO2 [16,17].

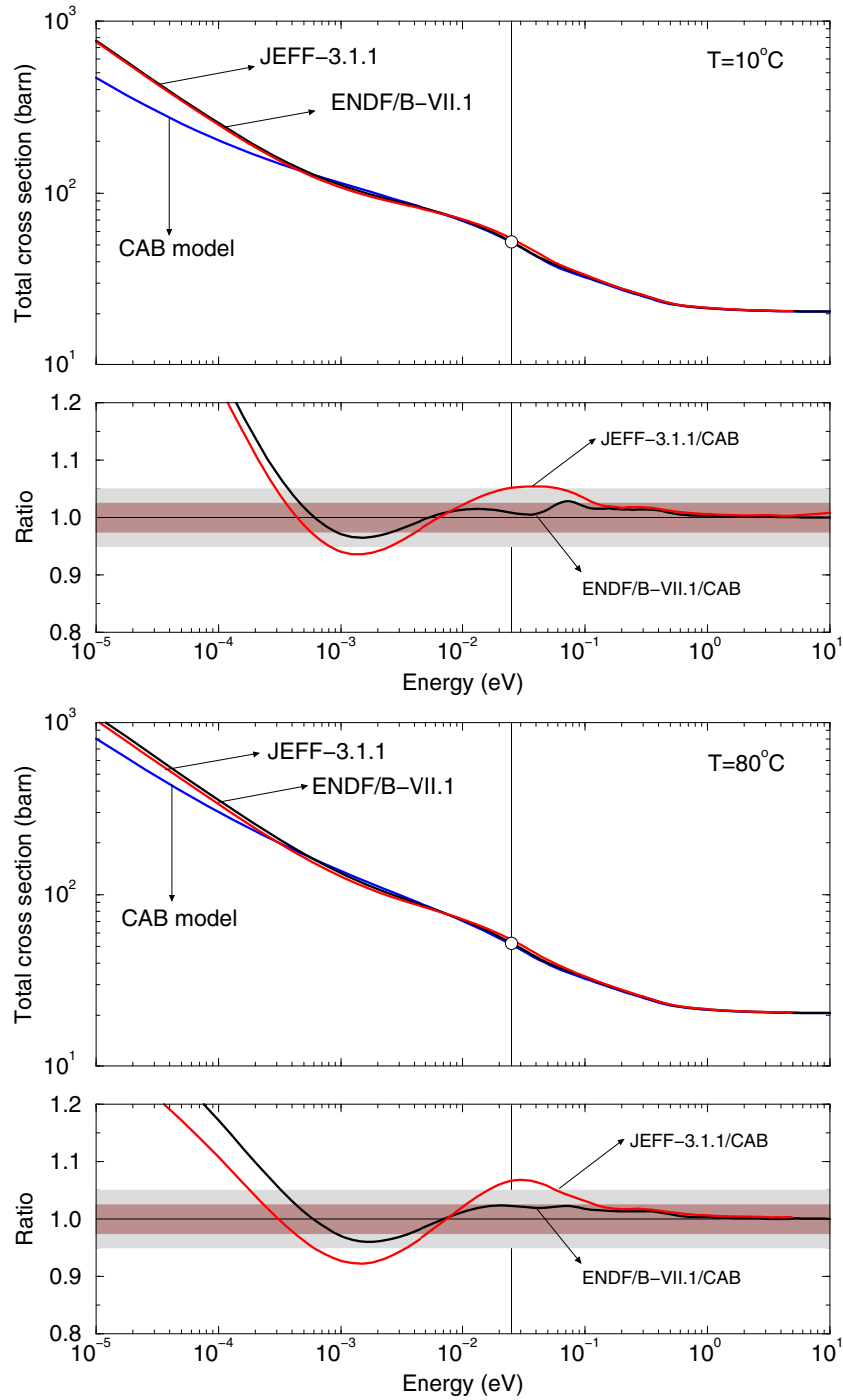


Fig. 8. Comparison of the total cross-sections of H in H_2O calculated at 10°C and 80°C . The discrepancy bands of $\pm 2.5\%$ and $\pm 5\%$ are shown to appreciate the discrepancy between the models.

4.3 Calculation errors on the reactivity temperature coefficient

The temperature effect on the reactivity can be expressed by the temperature coefficient α_{iso} , defined as the change in reactivity due to a change in temperature. The deviation

from the experimental values is given by the derivative of equation (12) with respect to the temperature:

$$\Delta\alpha_{iso}(T) = \sum_{i=1}^n ia_i T^{i-1} + \Delta\alpha_{cor}, \quad (13)$$

Table 4. Differences in reactivity $\Delta\rho = C - E$ (in pcm) obtained with the thermal scattering laws of JEFF-3.1.1, ENDF/B-VII.1 and calculated with the CAB model for the MISTRAL-1, MISTRAL-2 and MISTRAL-3 configurations. The statistical uncertainty due to the Monte-Carlo calculations is ± 2 pcm.

T (°C)	MISTRAL-1 (UOX)			MISTRAL-2 (MOX)			MISTRAL-3 (MOX)		
	JEFF-3.1.1	CAB model	ENDF/B-VII.1	JEFF-3.1.1	CAB model	ENDF/B-VII.1	JEFF-3.1.1	CAB model	ENDF/B-VII.1
6	206	295	273						
10	206	293	279	746	916	827	707	835	761
15				732	900	815			
20	192	283	258	732	900	815	657	788	717
25				727	903	811			
30	193	282	256	725	904	807	687	826	749
40	198	291	263	730	897	801	672	815	729
45				712	897	792			
50				705	889	790			
60	161	264	225	697	878	775	627	772	684
65	148	257	214	708	894	787			
70	128	240	199	690	872	766	614	768	673
75	127	232	195	686	860	763			
80	124	234	196	688	869	763	621	779	686

where $\Delta\alpha_{cor}$ is a correction factor introduced to account for the thermal expansion of the materials. Such a correction was applied in the previous interpretation of the MISTRAL-1 experiment with the deterministic code APOLLO2 [16]. In the present work, we decided to use a similar strategy for a better comparison of the MISTRAL-1 results.

Temperature variation produces a thermal expansion of the fuel pellet, clad and grid that will have an impact on the effective multiplication factor. The lattice pitch will increase with the temperature, modifying the moderation ratio. Consequently, the contribution of the resonance absorption will decrease and the resonance escape probability will increase. The aluminum overclad will have an opposite effect because its objective is to remove moderator, compensating the increase in the moderation ratio. UOX and MOX oxides have a lower thermal expansion coefficient than aluminum. They are characterized by a volume change of the order of 0.3% between 5 °C and 80 °C, which has a slight impact on the resonance absorption. For MISTRAL-1, the thermal expansion of the materials was calculated from a linear fit based on four temperatures (6 °C, 20 °C, 40 °C and 80 °C). The deduced correction is:

$$\Delta\alpha_{cor} = 0.9 \pm 0.1 \text{ pcm/}^\circ\text{C}.$$

The present result is twice as large as the correction found in the previous interpretations performed with the APOLLO2 code. Unfortunately, no obvious explanations were found for understanding the differences. For MISTRAL-2 and MISTRAL-3, the calculated reactivity includes the thermal dilatation effects and no correction is needed ($\Delta\alpha_{cor} = 0$).

The calculation errors on RTC are summarized in Table 7. Results are averaged over broad temperature intervals between the temperature T_1 and T_2 :

$$\Delta\alpha_{iso} = \sum_{i=1}^n a_i \frac{T_2^i - T_1^i}{T_2 - T_1} + \Delta\alpha_{cor}. \quad (14)$$

The present work provides the first interpretation of the RTC errors with the Monte-Carlo code TRIPOLI4[®]. Previous calculations were performed with the deterministic code APOLLO2. For the UOX configuration (MISTRAL-1), we observe differences of about 0.8 pcm/°C between the APOLLO2 and TRIPOLI4[®] results. The origin of such a systematic bias is hard to explain, especially since a better agreement is achieved for the MOX configurations (MISTRAL-2 and MISTRAL-3). However, results averaged over the broad temperature range [10 °C–80 °C] remain consistent with those reported in reference [17] and still confirm that the calculation errors are lower (UOX core) or nearly equal (MOX core) to the target accuracy of 1 pcm/°C:

$$\Delta\alpha_{iso}^{J311}(\text{UOX}) = -0.36 \pm 0.30 \text{ pcm/}^\circ\text{C}$$

$$\Delta\alpha_{iso}^{J311}(\text{MOX}) = -0.98 \pm 0.40 \text{ pcm/}^\circ\text{C}.$$

The comparison of the TRIPOLI4[®] results indicates that the thermal scattering laws of H in H₂O of the JEFF-3.1.1 and ENDF/B-VII.1 libraries provide similar $\Delta\alpha_{iso}(T)$ values. For the three MISTRAL configurations, no substantial differences can be observed between the calculation errors at low and high temperature, where spectral effects and water density effects dominate, respectively.

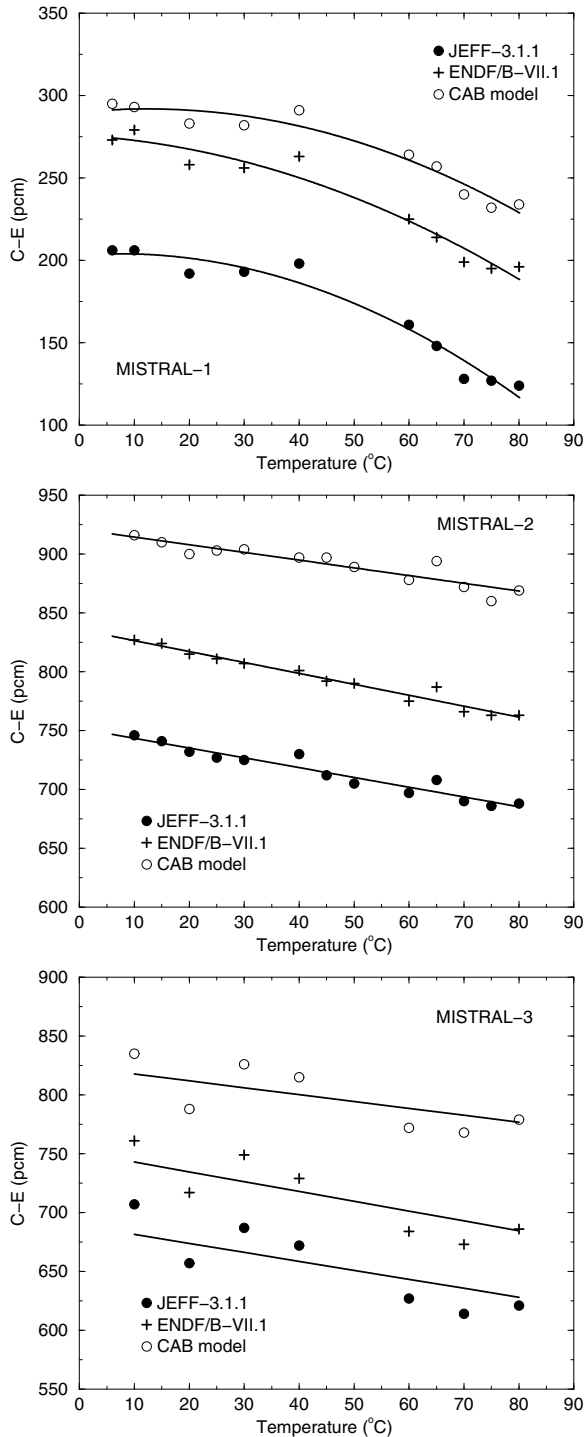


Fig. 9. Differences in reactivity $\Delta\rho(T)$ obtained with the thermal scattering laws of JEFF-3.1.1, ENDF/B-VII.1 and calculated with the CAB model for the MISTRAL-1, MISTRAL-2 and MISTRAL-3 configurations. The solid lines represent the best fit curves calculated with the CONRAD code [36].

For the UOX configuration, an improvement is achieved above 40 °C with the CAB model. As shown in Figure 10, this improvement reaches +0.6 pcm/°C at 80 °C. As a result, the calculation errors on RTC over the broad

temperature range [10 °C–80 °C] are close to zero when the thermal scattering law of H in H₂O from the CAB model is used:

$$\Delta\alpha_{iso}^{CAB}(\text{UOX}) = -0.02 \pm 0.30 \text{ pcm}/^\circ\text{C}.$$

For the MOX cores, the CAB model for H in H₂O leads to a substantial improvement of the calculation errors on RTC. Over the temperature range of interest, we obtain:

$$\Delta\alpha_{iso}^{CAB}(\text{MOX}) = -0.72 \pm 0.40 \text{ pcm}/^\circ\text{C}.$$

Although the magnitude of the improvement, close to +0.3 pcm/°C, is similar to the experimental uncertainty, it remains significant compared to the statistical uncertainty of +0.02 pcm/°C coming from the Monte-Carlo calculations. The observed differences between the CAB model and the other libraries are not due to a statistical bias. They point out a positive impact of the CAB model on the RTC calculations for MOX fuel.

The results reported for UOX fuel confirm the conclusions reported in reference [19] concerning the non-negligible contribution of the thermal scattering cross-section of Hydrogen on RTC calculations. Through the interpretation of the MISTRAL-1 configuration, we observe the impact of the thermal scattering laws of H in H₂O on the water density effects, increasing with the temperature. Such effects are of the same order of magnitude as the experimental uncertainties and their contributions to the calculation errors $\Delta\alpha_{iso}$ are similar to other nuclear data, such as the shape of the thermal cross-sections of the fissile isotopes [37,38].

5 Conclusions

A 3D model of the EOLE reactor by using the TRIPOLI4[®] Monte-Carlo code was used for the first time to achieve the interpretation of the RTC experiments performed in the MISTRAL-1, MISTRAL-2 and MISTRAL-3 configurations as a function of the temperature. This approach has not only confirmed previous results established with the deterministic code APOLLO2 but also provided new integral trends in relation with the thermal scattering laws of hydrogen bound to H₂O.

The comparison of the excess of reactivity calculated with three different sets of thermal scattering laws (JEFF-3.1.1, ENDF/B-VII.1 and CAB model) shows the impact of the intermolecular vibration modes of the water molecule in the neutron transport. The decrease of the translational mode in favor of the rotational mode leads to an increase of the calculated reactivity that can reach +180 pcm when the CAB model is used for the interpretation of the MISTRAL-2 configuration (MOX fuel).

In the whole temperature range of interest for this work [10 °C–80 °C], the calculation error on RTC for a standard UOX lattice is close to -0.4 pcm/°C when the JEFF-3.1.1 library is used. Such a bias vanishes and becomes closer to zero ($\Delta\alpha_{iso} = -0.02$ pcm/°C) when the thermal scattering laws are replaced by those generated

Table 5. Final Chi-square values provided by the CONRAD code [36] after the least-squares adjustment of the $\Delta\rho$ values reported in Table 4 with equation (12) for $n = 1, 2, 3$.

MISTRAL configuration	TSL data	Degree of the polynomial		
		$n = 1$	$n = 2$	$n = 3$
MISTRAL-1 (UOX)	JEFF-3.1.1	251.4	106.1	105.9
	ENDF/B-VII.1	180.4	124.8	122.7
	CAB model	184.3	81.9	84.1
MISTRAL-2,3 (MOX)	JEFF-3.1.1	560.3	561.5	631.0
	ENDF/B-VII.1	481.8	481.5	614.5
	CAB model	596.4	593.3	693.0

Table 6. Polynomial coefficients a_i provided by the CONRAD code [36] after the least-squares adjustment of the $\Delta\rho$ values reported in Table 4 with equation (12). Quadratic and linear polynomials are used for MISTRAL-1 and MISTRAL-2,3 respectively.

MISTRAL configuration	TSL data	Polynomial coefficients		
		a_0	a_1	a_2
MISTRAL-1 (UOX)	JEFF-3.1.1	203.2 ± 1.1	0.236 ± 0.023	-0.0164 ± 0.0004
	ENDF/B-VII.1	269.6 ± 1.1	0.222 ± 0.023	-0.0158 ± 0.0004
	CAB model	291.2 ± 1.1	0.250 ± 0.023	-0.0128 ± 0.0004
MISTRAL-2 (MOX)	JEFF-3.1.1	758.4 ± 1.1	-0.978 ± 0.188	–
	ENDF/B-VII.1	839.4 ± 1.1	-1.010 ± 0.188	–
	CAB model	924.0 ± 1.1	-0.722 ± 0.188	–
MISTRAL-3 (MOX)	JEFF-3.1.1	698.2 ± 1.5	-0.978 ± 0.188	–
	ENDF/B-VII.1	758.9 ± 1.5	-1.010 ± 0.188	–
	CAB model	829.6 ± 1.5	-0.722 ± 0.188	–

Table 7. Summary of the calculation errors $\Delta\alpha_{iso}$ (in pcm/°C) for the MISTRAL experiments obtained with the Monte-Carlo code TRIPOLI4[®]. Our results are compared with those obtained with the deterministic code APOLLO2 [17]. The experimental uncertainties are also given in pcm/°C. The contribution of the statistical uncertainties due to the Monte-Carlo calculations (± 0.02 pcm/°C) is negligible.

MISTRAL configuration	Temperature range	Exp. unc.	Calculation errors on RTC in pcm/°C			
			JEFF-3.1.1 (APOLLO2)	JEFF-3.1.1 (TRIPOLI4)	ENDF/B-VII.1 (TRIPOLI4)	CAB model (TRIPOLI4)
MISTRAL-1 (UOX)	10 to 40 °C	± 0.4	+0.9	+0.29	+0.31	+0.49
	40 to 80 °C	± 0.4	+0.1	−0.86	−0.80	−0.41
	10 to 80 °C	± 0.3	+0.4	−0.36	−0.33	−0.02
MISTRAL-2 (MOX)	10 to 40 °C	± 0.4	−0.5			
	40 to 80 °C	± 0.4	−1.1			
	10 to 80 °C	± 0.3	−0.9	−0.98	−1.01	−0.72
MISTRAL-3 (MOX)	10 to 40 °C	± 0.5	−0.4			
	40 to 80 °C	± 0.5	−1.4			
	10 to 80 °C	± 0.4	−1.0			

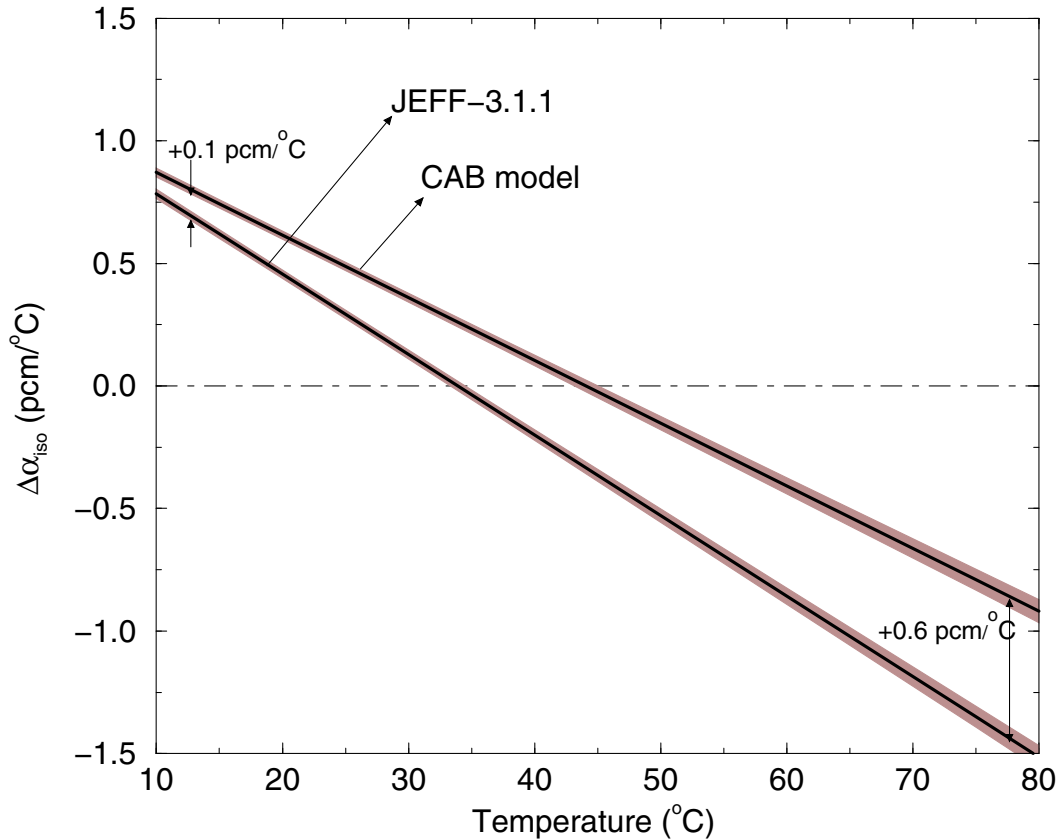


Fig. 10. Calculation errors on RTC as a function of the temperature for the MISTRAL-1 experiments. The uncertainty bands account for the statistical uncertainty of the Monte-Carlo calculations.

with the CAB model. This result indicates that the spectral component of the error in the RTC as well as the water expansion effects are well described. For MOX fuel configurations, the calculation error on RTC is of the order of -1.0 pcm/°C by using the JEFF-3.1.1 library. A similar trend is reached when the thermal scattering laws are replaced by those of the ENDF/B-VII.1 library. Our Monte-Carlo calculations show a slight reduction of the bias with the thermal scattering laws coming from the CAB model. The calculation error on RTC becomes closer to -0.7 pcm/°C. Such an improvement ($+0.3$ pcm/°C) is of the same order of magnitude as the uncertainty of the ^{239}Pu thermal cross-section shapes.

Results obtained with the CAB model aim at demonstrating the interest of using Molecular Dynamic simulations for producing reliable thermal scattering laws of hydrogen bound in light water. In cold operating conditions at atmospheric pressure, Molecular Dynamic simulations seem to provide better $S(\alpha, \beta)$ tables at temperatures where the change of water phase becomes relevant.

Thanks are addressed to Olivier Litaize and Yannick Peneliau, from the Nuclear Data group of CEA Cadarache, for the valuable discussions and their relevant advices during the interpretation of the MISTRAL programs with the Monte-Carlo code TRIPOLI4[®].

References

1. J.J. Duderstadt, L.J. Hamilton, *Nuclear Reactor Analysis* (Wiley and Sons, New York, 1976)
2. T. Zagar, M. Ravnik, *Kerntechnik* **70**, 223 (2005)
3. R.M. Gomes do Prado Souza, A.Z. Mesquita, *Prog. Nucl. Energy* **53**, 1126 (2011)
4. T. Bily, L. Sklenka, *Ann. Nucl. Eng.* **71**, 91 (2014)
5. M. Tsuji et al., *Nucl. Sci. Eng.* **43**, 576 (2006)
6. A. Santamarina, Thermal effects analysis in LWR lattices - Thermal cross-section shapes and qualification through French integral experiments, IAEA TECDOC-491, 1989 (see also CEA Rapport CEA-R-6215, 2009)
7. S. Cathalau et al., MISTRAL: an experimental program in the EOLE facility devoted to 100% MOX core physics, in *Proc. Int. Conf. on Physics of Reactors, PHYSOR 1996, Mito, Japan 1996*
8. T. Yamamoto et al., Core Physics experiment of 100% MOX core MISTRAL, in *Proc. Int. Conf. on Future Nuclear Systems, Yokohama, Japan, GLOBAL'97 (1997)*
9. S. Cathalau et al., First validation of neutronic lattice parameters of over moderated 100% MOX fueled PWR cores on the basis of the MISTRAL experiment, in *Proc. Int. Conf. on the Physics of Nuclear Science and Technology: future Nuclear Systems, Long Island, USA (1998)*
10. P. Fougeras et al., MISTRAL-4: an experimental mockup in the EOLE facility devoted to high moderation 100% MOX core Physics, in *Proc. Int. Conf. on the Future Nuclear Systems, GLOBAL'99, Jackson Hole, USA (1999)*

11. K. Hibi et al., Analysis of MISTRAL and EPICURE experiments with SRAC and MVP code systems, in *Proc. Int. Conf. Physics of Reactor Operation, Design and Computation, PHYSOR 2000, Pittsburg, USA* (2000)
12. M. Tatsumi et al., Analysis of High Moderation PWR MOX Core MISTRAL-4 with SRAC and MVP, in *Proc. Int. Conf. on Nuclear Data for Science and Technology, ND2001, Tsukuba, Japan* (2001)
13. T. Yamamoto et al., Analysis of MISTRAL Experiments with JENDL-3. 2, in *Proc. Int. Conf. on Nuclear Data for Science and Technology, ND2001, Tsukuba, Japan* (2001)
14. S. Cathalau et al., Full MOX recycling in ALWR: Lessons Drawn through the MISTRAL Program, in *Proc. Int. Conf. PHYSOR2002, Seoul, Korea* (2002)
15. O. Litaize et al., Analysis of the MISTRAL experiment with APOLLO2 qualification of neutronic parameters of UOX and MOX cores, in *Proc. Int. Conf. PHYSOR 2002, Seoul, Korea* (2002)
16. L. Erradi et al., *Nucl. Sci. Eng.* **144**, 47 (2003)
17. L. Erradi, A. Santamarina, Analysis of the MISTRAL experiment on the reactivity temperature coefficient for UOX and MOX lattices using JEFF-3. 1. 1 nuclear data library, in *Proc. Int. Conf. PHYSOR 2010, Advances in Reactor Physics to Power the Nuclear Renaissance, Pittsburgh, USA* (2010)
18. R. Sanchez et al., *Nucl. Sci. Technol* **42**, 474 (2010)
19. B.K. Jeon et al., *Nucl. Technol* **191**, 1 (2015)
20. E. Brun et al., *Ann. Nucl. Energy* **82**, 151 (2015)
21. A. Santamarina et al., The JEFF-3.1.1 Nuclear Data Library, JEFF Report 22, 2009
22. M.B. Chadwick et al., *Nucl. Data Sheets* **112**, 2887 (2011)
23. J.I. Marquez Damian et al., *Ann. Nucl. Energy* **65**, 280 (2014)
24. R.E. MacFarlane, New thermal neutron scattering files for ENDF/B-VI, Los Alamos National Laboratory Report, 1994
25. R.E. MacFarlane, A.C. Kahler, *Nucl. Data Sheets* **111**, 2739 (2010)
26. D.E. Cullen et al., How accurately we can calculate neutrons slowing down in water? Lawrence Livermore National Laboratory Report, UCRL-TR-220605, 2006
27. G. Vineyard, *Phys. Rev.* **110**, 999 (1958)
28. M. Mattes, J. Keinert, Thermal neutron scattering data for the moderator materials in ENDF-6 format and as ACE library for MCNP codes, International Atomic Energy Agency Report INDC(NDS)-0470, 2005
29. D.I. Page, B.C. Haywood, The Harwell scattering law program: frequency distributions of moderators, Harwell Laboratory Report AERE-R-5778, 1968
30. P. Egelstaff, P. Schofield, *Nucl. Sci. Eng.* **12**, 260 (1962)
31. G. Noguere, J-C. Sublet, *Ann. Nucl. Energy* **35**, 2259 (2008)
32. A. Santamarina et al., *Ann. Nucl. Energy* **48**, 51 (2012)
33. C. Lampoudis et al., *Eur. Phys. J. Plus* **128**, 86 (2013)
34. G. Noguere et al., *Phys. Rev. C* **92**, 014607 (2015)
35. G. Noguere et al., *Nucl. Sci. Eng.* (2016) (accepted for publication)
36. P. Archier et al., *Nucl. Data Sheets* **118**, 488 (2014)
37. D. Bernard et al., Pu nuclear data improvements in thermal and epithermal neutron ranges, in *Proc. Int. Conf. on Nuclear Data for Science and Technology, Nice, France* (2007)
38. C. De Saint Jean et al., Co-ordinated Evaluation of Plutonium-239 in the Resonance, Region, Nuclear Energy Agency Report WPEC/DOC(2014)447, 2014

Cite this article as: Juan Pablo Scotta, Gilles Noguere, David Bernard, Jose Ignacio Marquez Damian, Alain Santamarina, Impact of the thermal scattering law of H in H₂O on the isothermal temperature reactivity coefficients for UOX and MOX fuel lattices in cold operating conditions, EPJ Nuclear Sci. Technol. **2**, 28 (2016)